Engineering 58 (2026) 95–105

Contents lists available at ScienceDirect

Engineering

journal homepage: www.elsevier.com/locate/eng

Research
Recycling of Polymeric Materials—Article

Upcycling Polyethylene into Separable Aromatics Through Tandem Catalysis with CO_2 at Atmospheric Pressure

Wenjun Chen [a], Mingyu Chu [b], Yue Liu [a], Yiyi Fan [a], Meiqi Zhang [b,*], Meng Wang [b], Fan Zhang [a,*]

[a] National Engineering Laboratory of Eco-Friendly Polymeric Materials (Sichuan), College of Chemistry, Sichuan University, Chengdu 610064, China
[b] Beijing National Laboratory for Molecular Sciences, New Cornerstone Science Laboratory, College of Chemistry and Molecular Engineering, Peking University, Beijing 100871, China

ARTICLE INFO

Article history:
Received 28 February 2025
Revised 26 September 2025
Accepted 12 December 2025
Available online 17 December 2025

Keywords:
Polyethylene
CO_2
Tandem catalysis
Catalytic conversion
Aromatics

ABSTRACT

Selective conversion of two waste carbon resources—polyethylene and CO_2—into valuable chemicals through tandem catalysis offers a promising way to recover resources. However, current systems often have low selectivity for light aromatics in the liquid products, leading to mixtures of linear and cyclic compounds that are hard to separate. In this study, we developed a one-step process using an oxide–zeolite catalyst ($CuFeO_2$ + Ga-[Ga]/Zeolite Socony Mobil (ZSM)-5) at 400 °C and atmospheric pressure to produce separable liquid aromatics and CO from polyethylene and CO_2 at the same time. The synergistic effect between cationic Ga species and Brønsted acid sites in Ga-[Ga]/ZSM-5 promotes dehydrogenation while reducing typical hydrogen-transfer reactions, resulting in significant H_2 production. Meanwhile, the $CuFeO_2$ component supports the reverse water–gas shift reaction, shifting the reaction equilibrium and increasing the formation of aromatics through better hydrogen utilization. This cascade catalytic system achieves 99% selectivity toward separable aromatics in the liquid products and 91.9% toward C_1–C_2 aliphatic hydrocarbons in the gaseous products. The yield of aromatics reaches 75.3 weight percent (wt%), with benzene, toluene, and xylene making up 81.1% of this fraction. Additionally, CO_2 conversion reaches up to 10.9 mmol per gram of polyethylene. This strategy effectively turns waste plastics and CO_2 into valuable products, offering a practical approach for waste valorization and CO_2 utilization.

© 2025 THE AUTHORS. Published by Elsevier LTD on behalf of Chinese Academy of Engineering and Higher Education Press Limited Company. This is an open access article under the CC BY-NC-ND license (http://creativecommons.org/licenses/by-nc-nd/4.0/).

1. Introduction

Global plastic production has exceeded 9 billion metric tons, with polyethylene (PE) comprising the largest share [1]. Due to its durability and limited recyclability, most PE is discarded, leading to serious environmental issues [2,3]. Traditional waste management methods, such as incineration and landfilling, significantly increase carbon emissions and deplete fossil fuel resources [4,5]. Chemical recycling technologies offer a promising alternative by transforming waste PE into valuable chemicals. This approach not only addresses environmental concerns linked to plastic waste but also provides economic benefits [1,6,7]. However, the chemical recycling of PE remains challenging due to its strong C–C bonds, which typically require high temperatures, thereby reducing process efficiency and product selectivity [8,9].

To address these issues, various catalytic systems operated at lower temperatures have been developed (Fig. 1(a)). For example, supported noble-metal catalysts facilitate hydrogenolysis and hydrocracking of PE into linear and branched alkanes at 200–400 °C [10–15]. These alkane products can be used as components in gasoline or as lubricants. Alternatively, PE can be converted into olefins—mainly propylene—through combined dehydrogenation with alkene isomerization and metathesis [16,17], or into C_3–C_8 iso-olefins via β-cracking over zeolites at 280–350 °C [18]. However, the first method requires large amounts of the costly co-reactant (ethylene), while the second produces complex mixtures of products that hinder practical application. Additionally, tandem hydrogenolysis and aromatization can transform PE into alkyl-aromatic blends; nonetheless, the formation of numerous linear and cyclic by-products complicates separation [19]. There is an urgent need to develop processes that generate easily separable, highly selective, and high-value products from waste PE without depending on expensive co-reactants.

Light aromatics, such as benzene, toluene, and xylene (BTX), are vital petrochemical intermediates traditionally produced via

* Corresponding authors.
E-mail addresses: zhangmeiqi@pku.edu.cn (M. Zhang), fanzhang@scu.edu.cn (F. Zhang).

https://doi.org/10.1016/j.eng.2025.12.006
2095-8099/© 2025 THE AUTHORS. Published by Elsevier LTD on behalf of Chinese Academy of Engineering and Higher Education Press Limited Company.
This is an open access article under the CC BY-NC-ND license (http://creativecommons.org/licenses/by-nc-nd/4.0/).

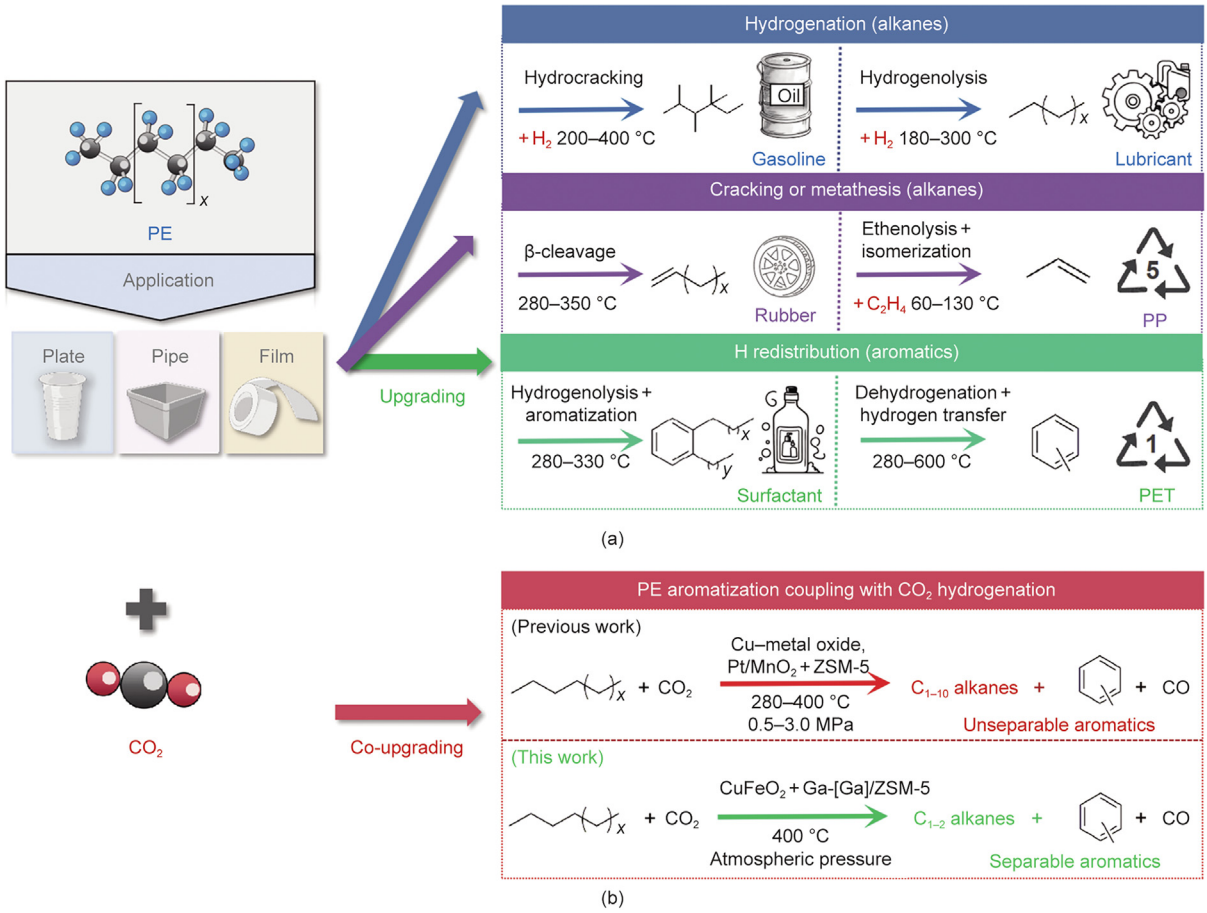

Fig. 1. (a) Schematic illustration of existing chemical recycling pathways for PE and co-reactants. (b) Comparison between previous methods and this approach for converting PE and CO_2 into aromatics. PP: polypropylene; PET: polyethylene terephthalate.

naphtha reforming [20–26]. Expanding feedstock options for aromatics production is becoming increasingly crucial, especially with the availability of waste PE [27,28]. From a molecular composition standpoint, based on its carbon-to-hydrogen ratio (C_nH_{2n}), converting PE to aromatics involves hydrogen transfer and dehydrogenation reactions, which release significant amounts of active hydrogen species [29,30]. Conversely, using CO_2 as an alternative waste carbon feedstock relies on a high-capacity process, since its conversion—usually through catalytic hydrogenation—requires large amounts of hydrogen [31]. Utilizing the *in-situ* hydrogen produced during PE aromatization to hydrogenate CO_2 offers a promising method to convert waste carbon into valuable fuels and chemicals, with minimal dependence on external hydrogen. Recently, bifunctional oxide–zeolite (OXZEO) catalysts have shown great potential in CO_2 hydrogenation [32]. These catalysts combine metal oxides and zeolites in a stepwise process: Metal oxides activate CO_2 and H_2, and then the intermediates migrate to zeolite acid sites for conversion into products such as light olefins or aromatics. Since the temperature ranges for CO_2 hydrogenation and catalytic PE depolymerization overlap (320–400 °C), this integrated system supports the combined process of PE waste depolymerization and CO_2 conversion.

Recent studies by our group [30] and Zhao et al. [33] have successfully converted both PE and CO_2 into valuable aromatics and CO using OXZEO-type catalytic systems. In these systems, CO_2 functions as a hydrogen scavenger through hydrogenation, reducing alkanes formation from hydrogenolysis or hydrogenation of intermediates and thereby boosting aromatization. Aromatics selectivity significantly surpassed the upper limit (about 50%) of traditional hydrogen-transfer pathways. Additionally, Pan et al. [34] reported a bifunctional OXZEO catalyst, Pt/MnO_x–Zeolite Socony Mobil (ZSM)-5, that facilitates PE aromatization in the presence of CO_2, achieving an aromatics yield of up to 64%, with BTX making up 60% of the products. Notably, 90% of the CO_2 used was incorporated into the aromatic products. However, these methods typically require high CO_2 pressures and show suboptimal BTX selectivity in the liquid phase, which increases separation costs and limits scalability. Therefore, there is significant potential to improve catalyst design and reaction conditions to boost catalytic activity and aromatics selectivity.

In this study, we developed a bifunctional composite catalyst composed of Ga-modified ZSM-5 zeolite (Ga-[Ga]/ZSM-5, where [Ga] indicates that Ga is incorporated into the framework of ZSM-5, which serves to distinguish it from that loaded onto the zeolite) and $CuFeO_2$ oxide, which effectively couples PE aromatization with CO_2 hydrogenation (Fig. 1(b)). Importantly, CO_2 accelerates aromatization by consuming H_2 generated from PE. Under optimal conditions (400 °C, zeolite-to-oxide ratio of 5, domino-type catalyst assembly), various waste polyolefins were selectively converted into separable gaseous alkanes (C_1–C_4) and liquid aromatics (C_6–C_{12}). To further improve the product distribution, a cascade catalytic system was designed to enhance the conversion of light alkanes, achieving a final aromatics yield of 75.3 weight percent (wt%) (with BTX comprising 81.1%) and CO_2 consumption of 10.9 mmol per gram of polyethylene (g_{PE}). The gaseous products showed high C_1–C_2 selectivity (91.9%), making them suitable for dry reforming to produce syngas. This integrated strategy offers a practical route for converting both CO_2 and PE into valuable syngas and separable aromatics.

2. Experimental section

2.1. Chemicals and materials

Tetrapropylammonium hydroxide (TPAOH, 25 wt% in aqueous solution) was supplied by Sinopharm Co., Ltd. (China). Tetraethyl orthosilicate (TEOS), aluminum chloride hexahydrate ($AlCl_3{\cdot}6H_2O$), copper nitrate ($Cu(NO_3)_2{\cdot}3H_2O$), gallium nitrate ($Ga(NO_3)_3{\cdot}9H_2O$), and iron nitrate nonahydrate ($Fe(NO_3)_3{\cdot}9H_2O$) were obtained from Shanghai Titan Scientific Co., Ltd. (China). Ammonium fluoride (NH_4F) was purchased from Chengdu Kelong Chemical Co., Ltd. (China). Gases, including Ar, CO_2, and He, were provided by Runtai Special Gas Co., Ltd (China). Deionized water (resistivity = 18.25 MΩ·cm) was produced using an ultrapure water system.

2.2. Catalyst preparation

2.2.1. Direct hydrothermal synthesis of [Ga]/ZSM-5

A total of 20 g of TEOS was added to 28.1 g of TPAOH solution and stirred until complete hydrolysis was achieved. The resulting mixture was transferred to a 100 mL Teflon-lined stainless-steel autoclave and maintained at 70 °C for 72 h to obtain the seed solution. Subsequently, a mixed silicon source consisting of 20 wt% seed solution and 8 g of TEOS was added to a solution composed of 4.37 g of TPAOH solution and 12 g of deionized water. Aqueous solutions of $AlCl_3{\cdot}6H_2O$, $Ga(NO_3)_3{\cdot}9H_2O$, and NH_4F were introduced into the mixture, maintaining a Si/Al/Ga ratio of 40/1/1. The solution was transferred into a Teflon-lined stainless-steel autoclave and subjected to hydrothermal treatment in a rotating oven at 30 r·min^{-1} and 170 °C for 72 h. After cooling to room temperature, the product was washed, dried, and calcined in a muffle furnace at 550 °C for 6 h with a heating rate of 5 °C·min^{-1}. The actual Ga loading in [Ga]/ZSM-5 was determined to be 2.2 wt% by inductively coupled plasma-atomic emission spectroscopy (ICP-AES).

2.2.2. Synthesis of Ga-[Ga]/ZSM-5 via the wet impregnation method

Gallium nitrate ($Ga(NO_3)_3{\cdot}9H_2O$, 3 wt%) was dissolved in deionized water and added dropwise onto 1 g of [Ga]/ZSM-5 support. The mixture was sonicated for 1 h, allowed to stand overnight, and dried for 12 h. Reduction was performed under a 5% H_2/Ar atmosphere at 575 °C (5 °C·min^{-1}, 2 h), followed by re-oxidation in flowing air at 500 °C (1 °C·min^{-1}, 4 h) to obtain the Ga-[Ga]/ZSM-5 sample. Cu-[Ga]/ZSM-5, Fe-[Ga]/ZSM-5, and CuFe-[Ga]/ZSM-5 were prepared using the same procedure with the corresponding metal precursors. The actual Ga loading in Ga-[Ga]/ZSM-5 was 4.8 wt% as determined by ICP-AES.

2.2.3. Synthesis of $CuFeO_2$ via the co-precipitation method

Solution A was prepared by dissolving 2.42 g of $Cu(NO_3)_2{\cdot}3H_2O$ and 4.04 g of $Fe(NO_3)_3{\cdot}9H_2O$ in 40 mL deionized water under stirring. Solution B was prepared by dissolving 8 g of NaOH in 40 mL deionized water. Solution B was added dropwise to solution A under continuous stirring. After 30 min, 1 mL of propanal was introduced as a reducing agent. The mixture was transferred to a 100 mL Teflon-lined stainless-steel autoclave and maintained at 180 °C for 24 h. The product was collected by centrifugation, thoroughly washed, and then dried. Prior to the catalytic reaction, the catalyst was pre-reduced under 5% H_2 at 400 °C for 2 h.

2.3. Characterization

X-ray diffraction (XRD) patterns were obtained using a Shimadzu XRD-6100 diffractometer (Japan) with Cu Kα radiation (λ = 1.5406 Å), operated at 40 kV and 30 mA. N_2 adsorption–desorption measurements were performed using a JW-BK200 analyzer (JWGB Instruments, China) to determine the specific surface area and pore volume. Samples were pretreated at 350 °C for 12 h under vacuum. Transmission electron microscopy (TEM) and high-resolution TEM (HRTEM) were performed on a Tecnai G^2 F30 microscope (FEI Company, USA) at an acceleration voltage of 200 kV. Elemental composition was determined via inductively coupled plasma optical emission spectroscopy/mass spectrometry (ICP-OES/MS) using an Agilent 5800 instrument (USA). CO_2 temperature-programmed desorption (CO_2-TPD) was performed on an iChem-700 chemical adsorption instrument (PhysiChem Instruments Ltd., China). Samples were pretreated in He at 400 °C for 1 h, then cooled to room temperature, exposed to CO_2, purged with He, and subsequently heated to 800 °C at a rate of 10 °C·min^{-1}, with desorption monitored via a thermal conductivity detector (TCD). Pyridine (Py) and 2,6-di-*tert*-butylpyridine (DTBPy) adsorption infrared spectra were recorded using a Nicolet iS50 FT-IR spectrometer (Thermo Fisher Scientific, USA). Samples were pressed into self-supported wafers, activated at 400 °C under vacuum (2×10^{-2} Torr, 1 Torr ≈ 133.3224 Pa) for 2 h, cooled to 150 °C, exposed to probe molecule vapor for 30 min, evacuated, and then scanned. Diffuse reflectance infrared Fourier transform (DRIFT) spectroscopy was carried out with a Nicolet iS50 spectrometer, equipped with an *in-situ* diffuse reflectance cell (Harrick) and a mercury cadmium telluride (MCT) detector. The catalyst and PE were separated inside the cell by quartz wool. Background measurements were performed at 180 °C to examine the plastic's glass transition behavior, ensuring that its phase change did not affect the reaction analysis.

2.4. Catalytic performance evaluation

Reactions took place in a horizontal quartz tube reactor with an inner diameter of 9 mm and a length of 450 mm. High-density polyethylene (HDPE) powder (purchased from China Petroleum and Chemical Corporation, weight-average molecular weight (M_w) ≈160 000, as shown in Fig. S1 in Appendix A) and catalysts were loaded into the reactor, separated by quartz wool. The system was purged with Ar or CO_2 at a flow rate of 10 mL·min^{-1} for 30 min. During the reaction, a carrier gas mixture of 95% CO_2 and 5% Ar at 10 mL·min^{-1} was used. The reactor was heated to 400 °C at a rate of 40 °C·min^{-1} and maintained at this temperature for the required time. Effluent gases passed through a dry ice-cooled cold trap to collect liquids, while non-condensable gases were collected in a gas bag.

Liquid and gaseous products were quantified using *n*-dodecane and CH_4/He as internal standards, respectively. Liquid products were analyzed by gas chromatography (GC; Agilent 8860, USA) equipped with a flame ionization detector (FID) using a DB-5 column (30 m × 0.32 mm). The GC oven temperature was initially held at 40 °C for 3 min, then increased to 200 °C at a rate of 5 °C·min^{-1}, followed by a rise to 250 °C at 20 °C·min^{-1}, and finally held for 10 min. The injector and detector temperatures were 320 and 300 °C, respectively. High-purity N_2 was used as the carrier gas. Liquids were also characterized using nuclear magnetic resonance (NMR) spectroscopy (Bruker AVIII HD 400, Germany). Gaseous products were analyzed by GC (Shimadzu GC2014, Japan) equipped with a TCD and an FID. CO, CH_4, and H_2 were analyzed on TCD, while C_1–C_5 hydrocarbons were analyzed on FID using a PLOT-Al_2O_3 column (30 m × 0.32 mm). TCD and FID temperatures were set to 260 °C.

All catalytic tests were performed in duplicate to determine average values and error ranges.

Liquid products yield (Y_{liquid}) was calculated as

$$Y_{liquid} = \frac{\sum m_i \times f \times A_s/A_i}{m_{PE}} \times 100\% \quad (1)$$

where m_i is the mass of internal standard (*n*-dodecane); f is the relative correction factor; A_i and A_s are the peak areas of the internal standard and products, respectively; and m_{PE} is the mass of the initial reactant PE.

Gaseous products yield (Y_{gas}) was calculated as

$$Y_{gas} = \frac{\sum n_i \times M_s \times f \times A_s/\Delta A_i}{m_{PE}} \times 100\% \quad (2)$$

where n_i is the moles of internal standard (CH_4/He), M_s is the molar mass of the products, and ΔA_i denotes the difference in peak area before and after the addition of the internal standard. Since the gas product contains a small amount of methane, a sample must be injected into the GC before adding the internal standard to quantify the inherent methane and obtain its actual peak area.

Selectivity (S) for the aromatics and alka(e)nes was calculated as

$$S = \frac{\sum m_{AR/ALKA(E)}}{\sum m_P} \times 100\% \quad (3)$$

where $m_{AR/ALKA(E)}$ is the mass of aromatics and alka(e)nes and m_P is the mass of the detected products.

Residual coke and solids ($Y_{C\&S}$) were quantified by thermogravimetric analysis (TGA; TGA 55, TA Instruments, USA):

$$Y_{C\&S} = \frac{m_{C\&S}}{m_{PE}} \times 100\% \quad (4)$$

where $m_{C\&S}$ is the mass of residual coke and solids.

Since isotope labeling experiments confirm that CO_2 participates exclusively in the reverse water–gas shift (RWGS) reaction, the CO_2 consumption (C_{CO_2}) is defined as the ratio of detected CO moles (n_{CO}) to the mass of feedstock PE, representing the amount of CO_2 convertible per unit mass of PE (i.e., mol per g_{PE}):

$$C_{CO_2} = \frac{n_{CO}}{m_{PE}} \quad (5)$$

^{13}C isotope labeling experiments were conducted using $^{13}CO_2$ or $^{12}CO_2$ with unlabeled PE. Gas products were analyzed using a GC with a 5 Å molecular sieve column and detected by mass spectrometry (MS; OmniStar GSD 320, Pfeiffer Vacuum, Germany).

The regeneration process involved calcining the zeolite in air at 600 °C for 4 h to remove carbon deposits.

3. Results and discussion

3.1. Effects of catalyst composition on catalytic performance

We first investigated the depolymerization of PE coupled with the CO_2 reaction using various catalysts at 400 °C. A gas mixture containing 5% Ar and 95% CO_2 was used to transport molten PE to the catalyst bed, which consisted of either pure zeolite or a zeolite–oxide composite. This mixture also carried the resulting products to a cold trap and gas collection system (Fig. 2(a)). Detailed characterization of the zeolite and oxide components is available in Appendix A (Table S1 and Figs. S2–S6). After the reaction, the gaseous, liquid, and solid residues were systematically collected and analyzed as detailed in the experimental section.

Figs. 2(b) and (c), along with Table S2 in Appendix A, display the product yields and selectivity for various catalysts. The hydrogen form of ZSM-5 (HZSM-5) showed the lowest yield and selectivity toward aromatics. In contrast, [Ga]/ZSM-5 (prepared through *in-situ* synthesis) achieved an aromatics yield of 32.5 wt% and a selectivity of 47.0%, along with notable H_2 production. These findings suggest that introducing Ga significantly boosts the dehydrogenation activity of the catalyst [35]. As shown in Fig. S6, under conditions of incomplete PE conversion, the [Ga]/ZSM-5 catalyst also demonstrated a higher conversion rate. This enhancement is due to the formation of new Brønsted acid sites (BAS, framework Ga) and Lewis acid sites (LAS) caused by incorporating Ga into the zeolite framework (Table S3 and Fig. S7 in Appendix A). Increased acidity generally leads to higher cracking rates and improved aromatization activity [36].

To further enhance aromatics yield and selectivity, a Ga-[Ga]/ZSM-5 catalyst was prepared through redox treatment. Previous studies suggest that such treatment helps combine LAS with framework Ga species, lowering the energy barrier for olefin dimerization on BAS and encouraging deprotonation [37]. Experimental results show that, although the Ga-[Ga]/ZSM-5 catalyst had slightly reduced conversion, both aromatics yield and selectivity improved. During this process, cationic Ga species replaced some BAS, decreasing the overall BAS density. Yet, the catalytic performance of Ga-[Ga]/ZSM-5 still exceeded that of ZSM-5, mainly because LAS could effectively activate C–H bonds in long HDPE chains, promoting carbocation formation and boosting activity through LAS and BAS synergy [36]. Additionally, Ga-[Ga]/ZSM-5 had the highest LAS concentration, leading to a lower Brønsted-to-Lewis (B/L) acid site ratio. Its LAS facilitated HDPE dehydrogenation, significantly reducing alkane byproducts formation via hydrogen transfer, thereby enhancing aromatics selectivity and producing H_2 at a rate of 2.1 mmol·g_{PE}^{-1} (Fig. 2(d)).

However, zeolite catalysts alone are largely ineffective for CO_2 conversion during PE transformation, primarily due to their weak CO_2 adsorption capacity. This was further corroborated by CO_2-TPD experiments (Fig. S8 in Appendix A), which showed that the zeolite catalysts exhibit mainly physisorption of CO_2 below 210 °C. Introducing $CuFeO_2$ to the highly dehydrogenative Ga-[Ga]/ZSM-5 catalyst increased CO_2 consumption to 1.7 mmol·g_{PE}^{-1} (Fig. S9 in Appendix A). Additionally, the composite catalytic system (metal oxide + zeolite) further improved reaction rates and aromatization activity, resulting in higher yield and selectivity of aromatics compared to Ga-[Ga]/ZSM-5 alone (Fig. 2(d) and Fig. S7).

The influence of the reaction atmosphere was then further studied. As shown in Fig. 2(e), time-evolution experiments were performed in different atmospheres to thoroughly analyze the PE conversion process involving CO_2. During the first 10 min, the amount of recoverable products increased significantly under the catalysis of Ga-[Ga]/ZSM-5 and $CuFeO_2$. As the reaction continued, the PE conversion rate gradually decreased. However, the data clearly show that the reaction proceeds faster in the presence of CO_2. Under conditions of lower conversion, CO_2 was found to enhance reaction rates by about 25% on average. This acceleration is likely due to increased consumption of H_2 produced on the zeolite, aided by the oxide. In dehydrogenation–aromatization processes, H_2 removal is often a rate-limiting step in producing aromatics from olefin intermediates. Metallic active sites accelerate the reaction by enhancing H_2 consumption. Additionally, as shown in Fig. S10 in Appendix A, carbon deposit formation was slightly reduced under CO_2 conditions.

To further investigate the role of $CuFeO_2$, transition metals (Cu and Fe), known for activating CO_2, were added to [Ga]/ZSM-5. However, this modification reduced catalytic activity compared to unmodified [Ga]/ZSM-5 (Fig. S11 in Appendix A). The degradation of PE is closely linked to the external acidity of the zeolite [18]. Fourier transform infrared spectroscopy (FTIR) with DTBPy showed a significant decrease in external acid site peaks at 1610 cm^{-1}, dropping from 3.9 to 2.9 and 1.9 for Cu-[Ga]/ZSM-5 and Fe-[Ga]/ZSM-5, respectively, compared to [Ga]/ZSM-5 (Fig. S12 in Appendix A). The impregnation process also appeared to block some micropores in the ZSM-5 zeolite (Table S4 and Fig. S13 in Appendix A), resulting in reduced access to active sites and lower yield of aromatics. Therefore, combining metal oxides with zeolite is crucial for achieving optimal performance.

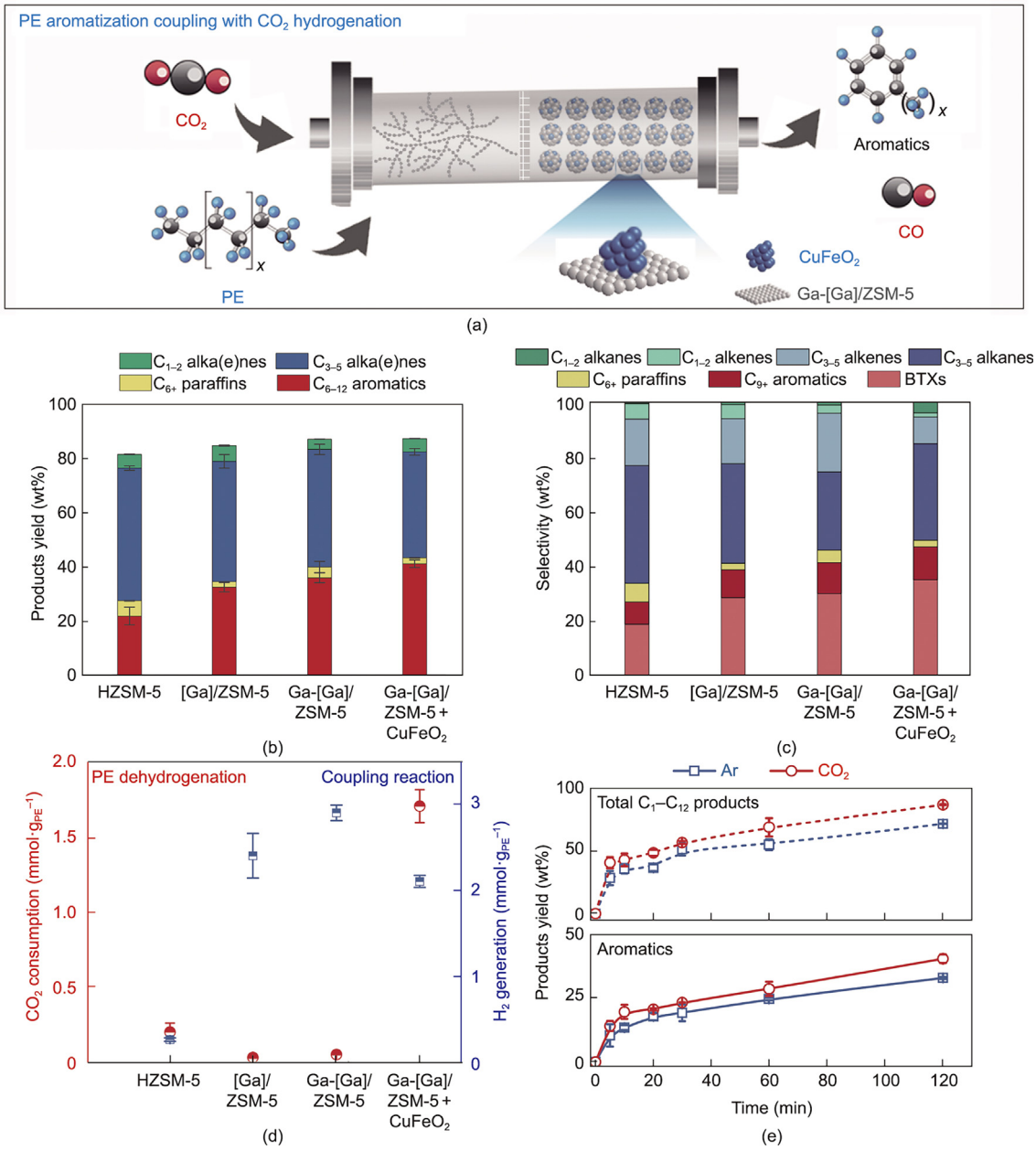

Fig. 2. (a) Schematic diagram of the reaction device. (b) Products yield and (c) selectivity on different catalysts in PE and CO_2 coupling reaction. (d) CO_2 consumption and H_2 production on different catalysts in PE and CO_2 coupling reaction. Reaction conditions: 0.1 g of $CuFeO_2$, 0.1 g of Ga-[Ga]/ZSM-5, 0.2 g of PE, 400 °C, atmospheric pressure, and 2 h. (e) Time evolution curves of products under different reaction atmospheres. Reaction conditions: 0.1 g of $CuFeO_2$, 0.1 g of Ga-[Ga]/ZSM-5, 0.2 g of PE, 400 °C, atmospheric pressure, and 5–120 min.

3.2. Effects of reaction conditions on the coupling reaction of PE with CO_2

We further investigated the effects of reaction temperature, the metal oxide-to-zeolite ratio, and the catalyst mixing method on the performance of the PE and CO_2 coupling reaction. The reaction was initially evaluated at temperatures between 350 and 450 °C, which exhibited a significant influence on process efficiency (Fig. 3(a), Table S5 and Fig. S14 in Appendix A). As shown in Fig. 3(a), increasing the temperature from 350 to 400 °C gradually raised the yield of recoverable products. This indicates that below 400 °C, PE undergoes limited cracking, while higher temperatures promote cracking and aromatization. As shown in Fig. S14, CO_2 consumption increases notably with rising temperature, highlighting the advantages of higher temperatures for the RWGS. When the temperature increased from 400 to 450 °C, aromatics yield only slightly improved from 23.5 to 26.1 wt%, and CO_2 consumption increased from 0.56 to 0.68 mmol·g_{PE}^{-1}. Since further temperature increases beyond 400 °C had a minimal effect on the formation of aromatics, we chose 400 °C as the test temperature for subsequent experiments.

As the metal oxide-to-zeolite ratio changed (Fig. 3(b), Table S6 and Fig. S15 in Appendix A), increasing the amount of zeolite in the composite catalyst resulted in more acidic sites, which enhanced PE conversion and aromatization. The higher aromatics yield indicated an increase in hydrogen-rich products, including H_2, consistent with the experimental results. Additionally, CO_2 consumption rose significantly—from 0.56 to 2.55 mmol·g_{PE}^{-1}—alongside a corresponding increase in aromatics yield—from 23.5 to 53.5 wt%.

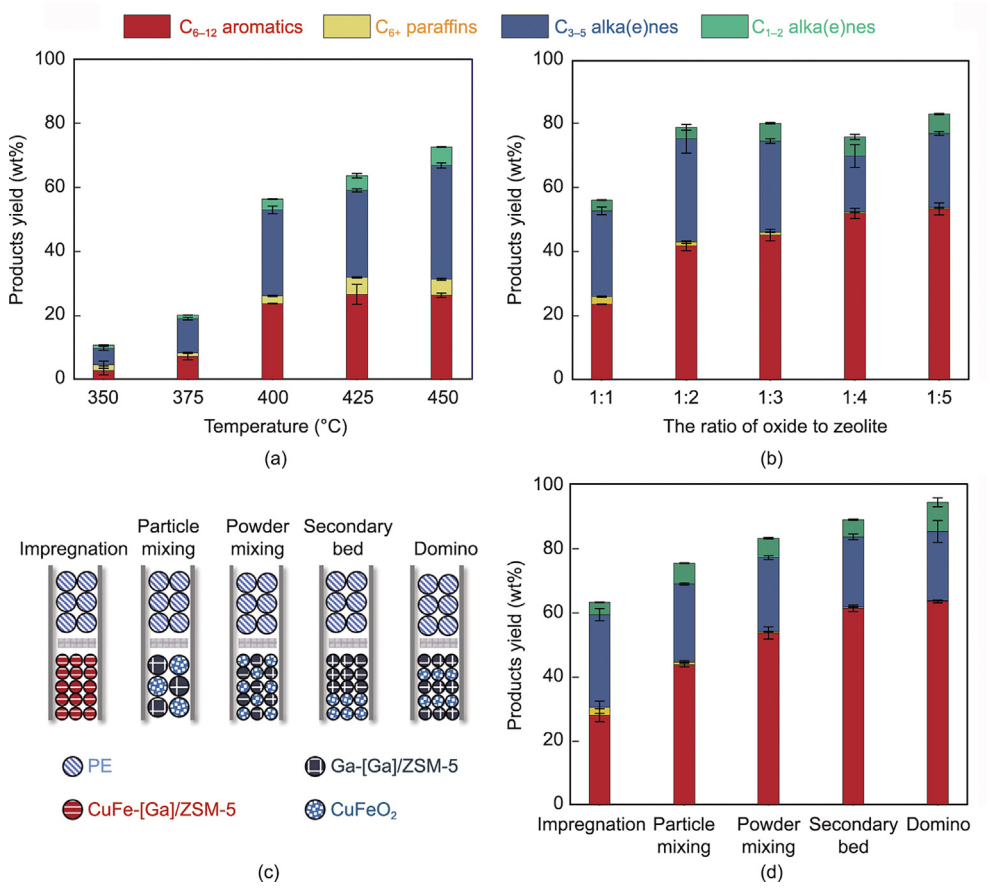

Fig. 3. Effects of reaction conditions on the catalytic performance of the tandem reaction of CO_2 and PE over Ga-[Ga]/ZSM-5 and $CuFeO_2$. (a) Effects of reaction temperature on products yield. (b) Effects of the ratio of oxide to zeolite on products yield. (c) Schematic diagram of catalyst assembly method. (d) Effects of catalyst assembly method on products yield. Reaction conditions: 0.1 g of $CuFeO_2$, 0.1–0.5 g of Ga-[Ga]/ZSM-5, 0.2 g of PE, 350–450 °C, atmospheric pressure, and 0.5 h.

Furthermore, we investigated how different catalyst assembly methods impact the performance of the bifunctional catalyst (Fig. 3(c), Table S7 and Fig. S16 in Appendix A). The nanoscale arrangement, particularly the deposition of metal oxide on Ga-[Ga]/ZSM-5, was found to reduce catalytic activity, resulting in the lowest aromatics yield and CO_2 consumption. The product yield of particle mixing was comparable to that of powder mixing; however, powder mixing resulted in a slight increase in both aromatics yield and CO_2 consumption. This is likely because a tubular reactor limits interactions between reactants and catalysts compared to an autoclave, thereby reducing the number of accessible active sites and limiting aromatics production. This is supported by the increased aromatics yield in secondary bed mode, although CO_2 consumption did not significantly rise. Therefore, we further developed a domino-type combination method, where H_2 produced from PE aromatization on the zeolite passes through multiple metal oxide beds, reacting with CO_2 to produce CO and maximizing both aromatics yield and CO_2 utilization.

3.3. Mechanism research in the coupling reaction of PE with CO_2

We further employed *in-situ* DRIFT to further investigate the mechanism of the coupling reaction of PE with CO_2 over Ga-[Ga]/ZSM-5 and $CuFeO_2$. As shown in Fig. 4(a), spectral bands appearing at 2930 and 1470 cm^{-1} as the reaction proceeds were attributed to asymmetric and symmetric CH_2 vibrations and C–H bending vibrations, respectively. These observations indicated that partially depolymerized PE gradually accumulated within the catalyst bed. Over time, compared to the CH_2 peak at 2930 cm^{-1}, the relative intensity of the CH_3 peak at 2963 cm^{-1} increased gradually, suggesting that the molecular weight of the accumulated products decreased. The skeletal vibrations of aromatic rings at 1501 cm^{-1} and the C–H stretching vibrations associated with aromatic rings at 3060 cm^{-1} confirmed the presence of aromatic compounds in the accumulated products on the catalyst. Meanwhile, the desorption/reaction of adsorbed species led to slight changes in the skeletal modes, resulting in three pseudo (derivative-type) bands in the 2050 to 1550 cm^{-1} spectral range [38,39]. The spectral bands in this region made it difficult to observe the formation of carboxylate species. However, the adsorption of CO bands (CO_{ad}) at 2080 and 1860 cm^{-1} was enhanced [33], along with the increasing characteristic vibration peaks of aromatics, confirming that the generated H_2 from the produced aromatics could gradually reduce CO_2 to CO.

We further conducted a ^{13}C isotopic labeling experiment by co-feeding $^{13}CO_2$. The GC–MS spectra of liquid- and gas-phase products from PE conversion under $^{13}CO_2$ atmosphere (Figs. 4(b) and (c)) confirm that $^{13}CO_2$ did not direct integration into hydrocarbon structures, consistent with our previous work [30]. Instead, only the RWGS reaction occurred, while other pathways such as CO_2 methanation [40], CO_2-Fischer–Tropsch synthesis [41], the coupling of CO_2 to methanol and then methanol to hydrocarbons [42], as well as the coupling of CO_2 to ketene and ketene to hydrocarbons, were excluded from the process [43]. Therefore, we propose the following CO_2-assisted reaction pathway for PE. As shown in Fig. 4(d), PE undergoes β-scission predominantly over the zeolite catalyst, generating short-chain olefins [34]. The synergistic interplay between LAS and BAS in Ga-[Ga]/ZSM-5 promotes dehydrogenation pathways while suppressing conventional

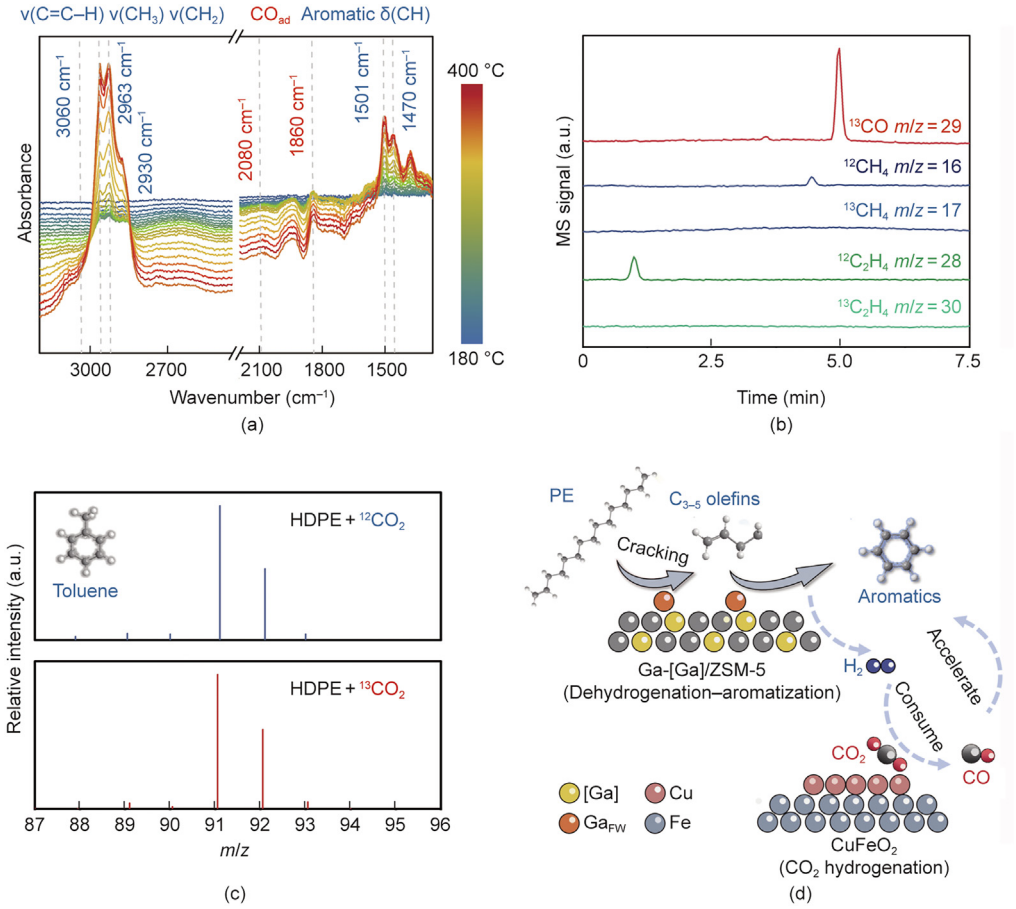

Fig. 4. Mechanistic understanding of the tandem reaction of PE with CO_2. (a) Operational DRIFT spectroscopy characterization of the coupling reaction of PE with CO_2. (b) MS spectra of gas products in the coupling reaction of PE with $^{13}CO_2$. (c) Contrast of MS spectra of liquid products in the coupling reaction of PE with $^{13}CO_2$ (red) and $^{12}CO_2$ (blue). Reaction conditions: 0.05 g of $CuFeO_2$, 0.05 g of Ga-[Ga]/ZSM-5, 0.1 g of PE, 400 °C, atmospheric pressure, and 1 h. (d) Proposed mechanism for the coupling reaction of CO_2 with PE over the composite catalyst at atmospheric pressure. CO_{ad}: the adsorption of CO bands; *m*/*z*: mass/charge ratio; Ga_{FW}: frameword Ga.

hydrogen-transfer reactions. However, the hydrogen formation step during olefin aromatization remains kinetically challenging, likely representing the rate-limiting step in the conversion of olefins to aromatics. Upon introducing CO_2, the hydrogen consumption mechanism is altered due to CO_2's direct participation and its conversion to CO and H_2O via the RWGS reaction over the oxide catalyst. This modification reduces the kinetic barrier for H_2 formation, thereby enhancing aromatics production [44]. Notably, no competitive adsorption phenomena were observed in this bifunctional catalyst system, likely due to the synergistic interaction between the dual active components.

3.4. Robustness of the catalytic system in the coupling reaction of PE with CO_2

To assess the stability of the catalyst system, we evaluated its catalytic performance on HDPE during the initial 10 min, when the PE was incompletely converted at 400 °C over four cycles. After collecting the products from this reaction, we extended the reaction time until full conversion for another cycle. As illustrated in Fig. 5(a), even after four consecutive uses of the catalyst (U-1 to U-4), there was no observable decline in reaction activity. The overall yield of both volatile compounds remained relatively constant throughout these trials. The recyclability of the catalyst was further examined by calcining the used zeolite in air at 600 °C. Remarkably, we observed no loss of activity even after multiple regenerations (R-1 and R-2), indicating strong resistance to irreversible deactivation and suggesting a robust catalyst framework. This observation aligns with the mostly stable porous structure and crystal phase of the zeolite and oxide components, as confirmed by Brunauer–Emmett–Teller (BET) and XRD analyses (Table S8 and Figs. S17 and S18 in Appendix A for details). Therefore, it is reasonable to expect that this catalyst system will have a long operational life and significant potential for applications in the co-conversion of PE and CO_2.

To further investigate the industrial application potential of the catalytic system, we evaluated its applicability using various real-world plastic products as feedstocks. We first tested disposable commercial PE plastics, including HDPE board and low-density polyethylene (LDPE) film, and the total yield of aromatics achieved ranged from 64.8 to 68.3 wt%, with CO_2 consumption varying between 2.4 and 4.0 mmol·g_{PE}^{-1}, as illustrated in Figs. 5(b) and (c). When commercial polypropylene (PP) plates were used, they yielded 60.0 wt% aromatics and consumed 4.2 mmol·g_{PE}^{-1} of CO_2 (Fig. 5(d)). It is important to note that actual plastic waste is often heterogeneous and may contain halides, such as polyvinyl chloride (PVC), which have the potential to poison active sites or compromise catalyst structures. Therefore, we also conducted coupling experiments on a mixture of plastics, comprising 30% HDPE, 30% LDPE, 20% PP, 13% polystyrene (PS), and 7% PVC. This experimentation resulted in a substantial yield of 57.8 wt% aromatics and CO_2 consumption of 3.6 mmol·g_{PE}^{-1} (Fig. 5(e)). It is noteworthy that all tested real-plastic feedstocks achieved an overall recovery rate over 80%, with concurrent aromatics selectivity over 90% in the

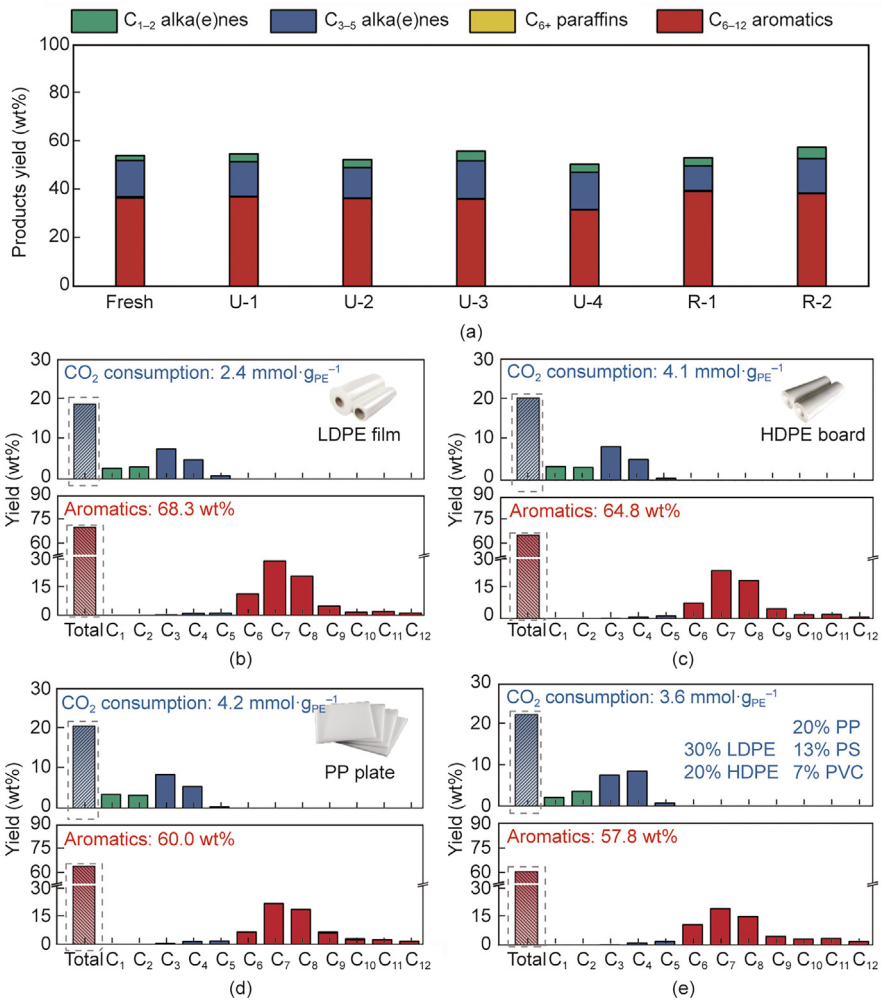

Fig. 5. Catalytic performance of $CuFeO_2$ and Ga-[Ga]/ZSM-5 in practical applications. (a) Recyclability test in the tandem reaction of PE and CO_2. Reaction conditions: 0.2 g of PE, 0.1 g of $CuFeO_2$, 0.5 g of Ga-[Ga]/ZSM-5, feed gas of 95% CO_2 and 5% Ar at 10 mL·min^{-1}, 10 min, 400 °C. U-1 to U-4 represent four consecutive cycles; R-1 and R-2 represent one regeneration and two regenerations, respectively. (b–e) Catalytic conversion of various polyolefins and mixed plastics: (b) LDPE film; (c) HDPE board; (d) PP plate; and (e) a mixture of plastics. Reaction conditions: 0.2 g of PE, 0.1 g of $CuFeO_2$, 0.5 g of Ga-[Ga]/ZSM-5, feed gas of 95% CO_2 and 5% Ar at 10 mL·min^{-1}, 1 h, 400 °C.

liquid product fraction (Figs. 5(b)–(e), Fig. S19 in Appendix A). These findings show that the catalytic system's robustness remains largely unaffected by changes in plastic density, branching, or typical impurities such as halogens.

3.5. Cascade catalysis to optimize product distribution

As confirmed, the coupled catalytic system proposed in this work converts diverse plastics into gaseous alkanes (C_1–C_4) and liquid aromatics (C_6–C_{12}). However, a fraction of C_3–C_4 alkanes remains in the liquid phase, which impairs aromatics selectivity and complicates product separation. To further improve product distribution, we implemented a cascade reactor with a second bed temperature of 550, 600, or 650 °C (Fig. 6(a)). Raising the temperature from 400 to 550 °C suppressed C_3–C_4 alkanes formation and increased aromatics yield to 67.5 wt%, while promoting cracking and aromatization (Fig. 6(b)). At 650 °C, aromatics yield reached 75.3 wt%, of which 81.1% was BTX (Figs. 6(b) and (c)). The higher temperature also enhanced CO_2 consumption (10.9 mmol·g_{PE}^{-1}) by accelerating the endothermic RWGS reaction.

As shown in Fig. 6(d) and Table S9 in Appendix A, the distribution of products reveals a typical bimodal pattern: C_1–C_2 aliphatic hydrocarbons mostly appear in the gas phase, while C_6–C_{12} aromatics mainly exist in the liquid phase. The selectivity reaches 92.7% for C_1–C_2 in gases and 99% for C_6–C_{12} aromatics in liquids. NMR analysis of the liquid product, illustrated in Fig. 6(e), shows the ^{13}C spectrum with aromatic (120–150 ppm) and aliphatic (10–30 ppm) signals, mostly from ring carbons. The hydrogen spectrum indicates most protons are linked to monocyclic aromatics (6.5–7.5 ppm) and their alkyl groups (2–3 ppm), with fewer on condensed rings (7.5–8.5 ppm). No signals appear in the aliphatic region (0–2 ppm), confirming the high purity of the aromatic-rich liquids. The ratio of protons associated with an aliphatic carbon directly bonded to an aromatic ring (C_α) to aromatic ring hydrogens (H_α/H_{aro}), as measured by GC–FID and ^1H NMR, was 0.53 and 0.60, respectively (Table S10 in Appendix A), indicating reliable and consistent data [19]. The small discrepancy likely results from trace multi-substituted C_{12+} aromatics that cannot be detected chromatographically. Additionally, carbon and hydrogen balances exceeded 95% for the catalytic PE conversion in CO_2, validating the accuracy and consistency of the data (Tables S11 and S12 and Fig. S20 in Appendix A).

Earlier studies on direct PE pyrolysis to produce aromatics often resulted in yields below 50 wt% within temperatures of 400–850 °C (Fig. 6(f), orange area) [28,45,46]. More recent methods, which combine conversion with CO_2 at lower temperatures (280–400 °C), have shown notable improvements, increasing the aromatics yield to around 60% (blue area). However, the selectivity

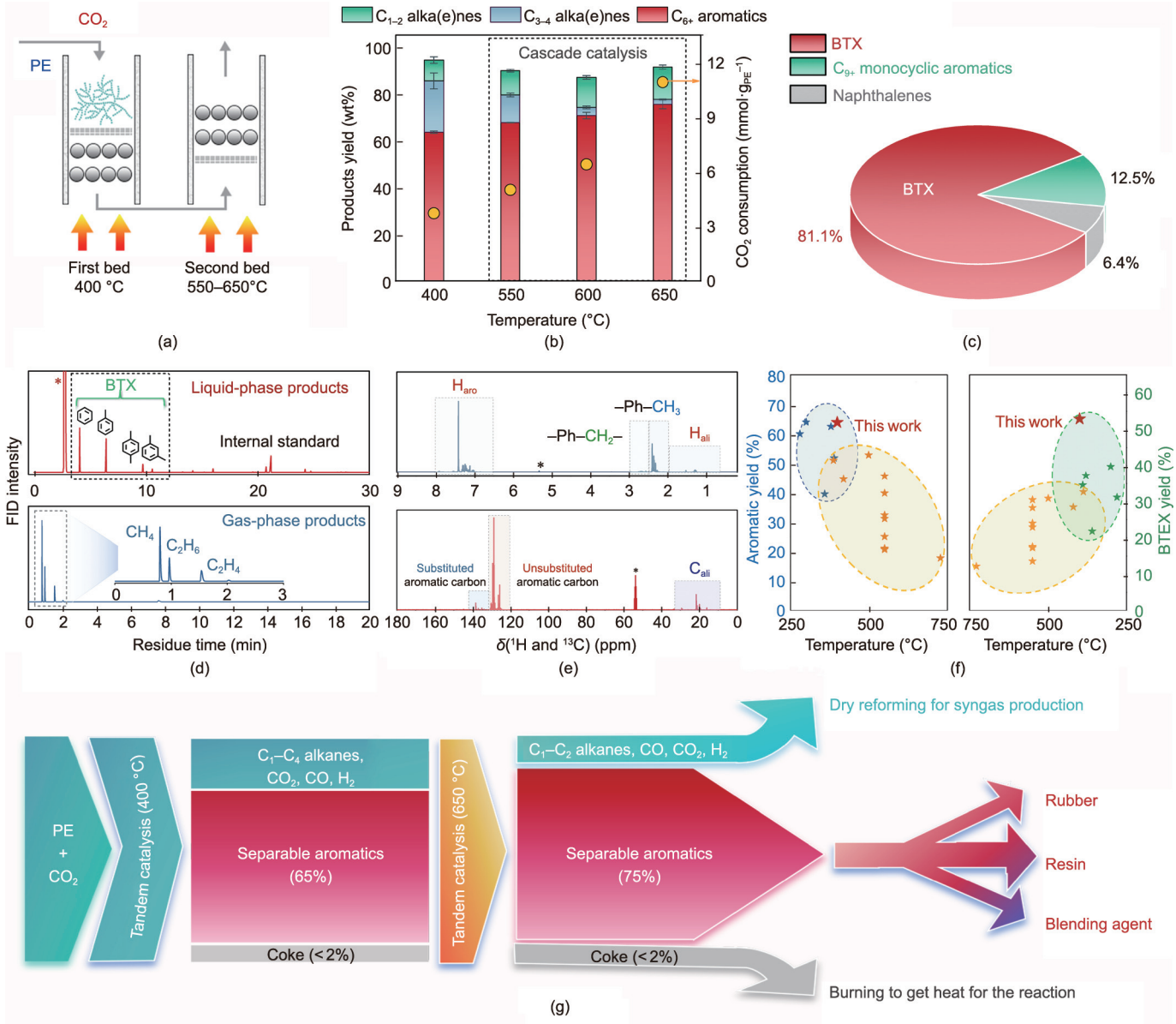

Fig. 6. (a) Schematic diagram of the proposed cascade catalysis reactor. (b) The effect of the second bed temperature on the tandem reaction of PE and CO_2. Reaction conditions: 0.2 g of PE, 0.1 g of $CuFeO_2$, and 0.5 g of Ga-[Ga]/ZSM-5 in the first bed; 0.1 g of $CuFeO_2$ and 0.5 g of Ga-[Ga]/ZSM-5 in the second bed; feed gas of 95% CO_2 and 5% Ar at 10 mL·min^{-1}, 2 h, and 550–650 °C. (c) Aromatics selectivity in the cascade catalysis reaction of PE and CO_2 at 650 °C in the second bed. (d) The GC spectra of gas products and liquid products in the cascade catalysis reaction of PE and CO_2 at 650 °C in the second bed. (e) ^{1}H NMR and ^{13}C NMR spectra of liquid products recorded in deuterated CD_2Cl_2. The symbol * represents the signal of the solvent. H_{aro}: aromatic hydrogens; H_{ali}: aliphatic hydrogens; C_{ali}: aliphatic carbons; Ph: phenyl. (f) Comparison of aromatics and benzene, toluene, ethylbenzene, and xylene (BTEX) yields with Refs. [20–28,30,33,34,45,46]. Blue and green areas represent the coupling conversion experiments of PE and CO_2. The orange area represents the traditional pyrolysis of PE to produce aromatic compounds. (g) Schematic representation of the carbon flow in the cascade catalysis reaction of PE and CO_2 and further utilization of the products.

for benzene, toluene, ethylbenzene, and xylene (BTEX) remains relatively low across these studies. The liquid products mainly contain cyclic hydrocarbons, alkanes, and aromatics with similar carbon numbers, making separation more difficult. The proposed cascade catalysis setup enables complete conversion of PE into a mixture of C_1–C_2 aliphatic hydrocarbons and C_6–C_{12} aromatics. According to the data, processing 1.0 kg of waste plastics with 0.48 kg of CO_2 produces about 0.75 kg of aromatics, 0.25 kg of fuel gas, and 0.31 kg of CO. Additionally, the fuel gas and CO_2 in the gases can undergo dry reforming to produce pure synthesis gas (Fig. 6(g)) [47]. This approach suggests that, in theory, PE and CO_2 can be fully converted into synthesis gas (CO + H_2) and liquid aromatics.

4. Conclusions

In summary, we developed an oxide–zeolite catalytic system ($CuFeO_2$ + Ga-[Ga]/ZSM-5) for the coupled conversion of polyolefins and CO_2 under atmospheric pressure. The system exhibited excellent activity and stability, increasing the reaction rate by approximately 25% compared to the CO_2-free reaction. We identified that the role of CO_2 is to enhance aromatics formation by consuming H_2 via the RWGS reaction, as confirmed by $^{13}CO_2$ isotopic labeling, which showed no incorporation of carbon from CO_2 into the aromatic products. Furthermore, a cascade catalysis strategy enabled the direct production of separable aromatics at a yield of 75.3 wt%, with BTX accounting for 81.1% of the total. This tandem

approach, integrating CO_2-assisted dehydrogenation with aromatization, offers a promising route for converting waste plastics into valuable liquid aromatics while mitigating greenhouse gas emissions.

CRediT authorship contribution statement

Wenjun Chen: Writing – original draft, Visualization, Validation, Investigation, Formal analysis, Data curation. **Mingyu Chu:** Validation, Methodology, Data curation. **Yue Liu:** Visualization, Formal analysis, Data curation. **Yiyi Fan:** Validation, Data curation. **Meiqi Zhang:** Validation, Supervision, Methodology, Formal analysis. **Meng Wang:** Methodology. **Fan Zhang:** Writing – review & editing, Supervision, Resources, Project administration, Methodology, Conceptualization.

Declaration of competing interest

The authors declare that they have no known competing financial interests or personal relationships that could have appeared to influence the work reported in this paper.

Acknowledgments

This work was financially supported by the National Key Research and Development Program of China (2021YFA1501700 and 2022YFA1504800), the Fundamental Research Funds from Sichuan University (2022SCUNL103), and the Funding for Hundred Talent Program of Sichuan University (20822041E4079). This work was partially supported by SINOPEC Research Institute of Petroleum Processing Co., Ltd. via collaborative project (36800000-24-ZC0607-0175).

Appendix A. Supplementary data

Supplementary data to this article can be found online at https://doi.org/10.1016/j.eng.2025.12.006.

References

[1] Sun J, Dong J, Gao L, Zhao YQ, Moon H, Scott SL. Catalytic upcycling of polyolefins. Chem Rev 2024;124(16):9457–579.
[2] Vollmer I, Jenks MJF, Roelands MCP, White RJ, van Harmelen T, de Wild P, et al. Beyond mechanical recycling: giving new life to plastic waste. Angew Chem Int Ed Engl 2020;59(36):15402–23.
[3] Geyer R, Jambeck JR, Law KL. Production, use, and fate of all plastics ever made. Sci Adv 2017;3(7):e1700782.
[4] Ma D. Transforming end-of-life plastics for a better world. Nat Sustain 2023;6(10):1142–3.
[5] Zhang MQ, Wang M, Sun B, Hu C, Xiao D, Ma D. Catalytic strategies for upvaluing plastic wastes. Chem 2022;8(11):2912–23.
[6] Martín AJ, Mondelli C, Jaydev SD, Pérez-Ramírez J. Catalytic processing of plastic waste on the rise. Chem 2021;7(6):1487–533.
[7] Gan L, Dong Z, Xu H, Lv H, Liu G, Zhang F, et al. Beyond conventional degradation: catalytic solutions for polyolefin upcycling. CCS Chem 2024;6(2):313–33.
[8] Anuar Sharuddin SD, Abnisa F, Wan Daud WMA, Aroua MK. A review on pyrolysis of plastic wastes. Energy Convers Manage 2016;115:308–26.
[9] Jung SH, Cho MH, Kang BS, Kim JS. Pyrolysis of a fraction of waste polypropylene and polyethylene for the recovery of BTX aromatics using a fluidized bed reactor. Fuel Process Technol 2010;91(3):277–84.
[10] Liu S, Kots PA, Vance BC, Danielson A, Vlachos DG. Plastic waste to fuels by hydrocracking at mild conditions. Sci Adv 2021;7(17):eabf8283.
[11] Cen Z, Han X, Lin L, Yang S, Han W, Wen W, et al. Upcycling of polyethylene to gasoline through a self-supplied hydrogen strategy in a layered self-pillared zeolite. Nat Chem 2024;16(6):871–80.
[12] Li L, Luo H, Shao Z, Zhou H, Lu J, Chen J, et al. Converting plastic wastes to naphtha for closing the plastic loop. J Am Chem Soc 2023;145(3):1847–54.
[13] Tu W, Chu M, Wang X, Wang X, Li Y, Yang W, et al. SMSI-induced charge transfer for selective hydrogenolysis of polyolefins. Appl Catal B 2023;339:123122.
[14] Nakaji Y, Tamura M, Miyaoka S, Kumagai S, Tanji M, Nakagawa Y, et al. Low-temperature catalytic upgrading of waste polyolefinic plastics into liquid fuels and waxes. Appl Catal B 2021;285:119805.
[15] Tennakoon A, Wu X, Paterson AL, Patnaik S, Pei Y, LaPointe AM, et al. Catalytic upcycling of high-density polyethylene via a processive mechanism. Nat Catal 2020;3(11):893–901.
[16] Conk RJ, Hanna S, Shi JX, Yang J, Ciccia NR, Qi L, et al. Catalytic deconstruction of waste polyethylene with ethylene to form propylene. Science 2022;377(6614):1561–6.
[17] Wang NM, Strong G, DaSilva V, Gao L, Huacuja R, Konstantinov IA, et al. Chemical recycling of polyethylene by tandem catalytic conversion to propylene. J Am Chem Soc 2022;144(40):18526–31.
[18] Duan J, Chen W, Wang C, Wang L, Liu Z, Yi X, et al. Coking-resistant polyethylene upcycling modulated by zeolite micropore diffusion. J Am Chem Soc 2022;144(31):14269–77.
[19] Zhang F, Zeng M, Yappert RD, Sun J, Lee YH, LaPointe AM, et al. Polyethylene upcycling to long-chain alkylaromatics by tandem hydrogenolysis/aromatization. Science 2020;370(6515):437–41.
[20] Gaurh P, Pramanik H. Production of benzene/toluene/ethyl benzene/xylene (BTEX) via multiphase catalytic pyrolysis of hazardous waste polyethylene using low cost fly ash synthesized natural catalyst. Waste Manag 2018;77:114–30.
[21] Zhang X, Lei H, Yadavalli G, Zhu L, Wei Y, Liu Y. Gasoline-range hydrocarbons produced from microwave-induced pyrolysis of low-density polyethylene over ZSM-5. Fuel 2015;144:33–42.
[22] Cho MH, Jung SH, Kim JS. Pyrolysis of mixed plastic wastes for the recovery of benzene, toluene, and xylene (BTX) aromatics in a fluidized bed and chlorine removal by applying various additives. Energy Fuels 2010;24(2):1389–95.
[23] Zhou N, Dai L, Lyu Y, Wang Y, Li H, Cobb K, et al. A structured catalyst of ZSM-5/SiC foam for chemical recycling of waste plastics via catalytic pyrolysis. Chem Eng J 2022;440:135836.
[24] Fu L, Xiong Q, Wang Q, Cai L, Chen Z, Zhou Y. Catalytic pyrolysis of waste polyethylene using combined CaO and Ga/ZSM-5 catalysts for high value-added aromatics production. ACS Sustain Chem Eng 2022;10(29):9612–23.
[25] Sun K, Wang W, Themelis NJ, Thanos Bourtsalas AC, Huang Q. Catalytic co-pyrolysis of polycarbonate and polyethylene/polypropylene mixtures: promotion of oil deoxygenation and aromatic hydrocarbon formation. Fuel 2021;285:119143.
[26] Wang Y, Cheng L, Gu J, Zhang Y, Wu J, Yuan H, et al. Catalytic pyrolysis of polyethylene for the selective production of monocyclic aromatics over the zinc-loaded ZSM-5 catalyst. ACS Omega 2022;7(3):2752–65.
[27] Xu D, Yang S, Su Y, Shi L, Zhang S, Xiong Y. Simultaneous production of aromatics-rich bio-oil and carbon nanomaterials from catalytic co-pyrolysis of biomass/plastic wastes and in-line catalytic upgrading of pyrolysis gas. Waste Manag 2021;121:95–104.
[28] Tian X, Zeng Z, Liu Z, Dai L, Xu J, Yang X, et al. Conversion of low-density polyethylene into monocyclic aromatic hydrocarbons by catalytic pyrolysis: comparison of HZSM-5, Hβ, HY and MCM-41. J Clean Prod 2022;358:131989.
[29] Serrano DP, Aguado J, Escola JM. Developing advanced catalysts for the conversion of polyolefinic waste plastics into fuels and chemicals. ACS Catal 2012;2(9):1924–41.
[30] Chen W, Jiao Y, Liu Y, Wang M, Zhang F, Ma D. One-pot upgrading polyethylene and CO_2 to aromatics via tandem catalysis. CCS Chem 2024;6(6):1422–9.
[31] Wei J, Yao R, Han Y, Ge Q, Sun J. Towards the development of the emerging process of CO_2 heterogenous hydrogenation into high-value unsaturated heavy hydrocarbons. Chem Soc Rev 2021;50(19):10764–805.
[32] Pan X, Jiao F, Miao D, Bao X. Oxide–zeolite-based composite catalyst concept that enables syngas chemistry beyond Fischer–Tropsch synthesis. Chem Rev 2021;121(11):6588–609.
[33] Liu Y, Ma B, Tian J, Zhao C. Coupled conversion of polyethylene and carbon dioxide catalyzed by a zeolite–metal oxide system. Sci Adv 2024;10(15):eadn0252.
[34] Ding Y, Zhang S, Liu C, Shao Y, Pan X, Bao X. CO_2-facilitated upcycling of polyolefin plastics to aromatics at low temperature. Natl Sci Rev 2024;11(5):nwae097.
[35] Gao P, Xu J, Qi G, Wang C, Wang Q, Zhao Y, et al. A mechanistic study of methanol-to-aromatics reaction over Ga-modified ZSM-5 zeolites: understanding the dehydrogenation process. ACS Catal 2018;8(10):9809–20.
[36] Gao P, Wang Q, Xu J, Qi G, Wang C, Zhou X, et al. Brønsted/Lewis acid synergy in methanol-to-aromatics conversion on Ga-modified ZSM-5 zeolites, as studied by solid-state NMR spectroscopy. ACS Catal 2018;8(1):69–74.
[37] Zhou Y, Thirumalai H, Smith SK, Whitmire KH, Liu J, Frenkel AI, et al. Ethylene dehydroaromatization over Ga-ZSM-5 catalysts: nature and role of gallium speciation. Angew Chem Int Ed Engl 2020;59(44):19592–601.
[38] Maggiulli L, Sushkevich VL, Kröcher O, van Bokhoven JA, Ferri D. Correlating the nature of carbenium ions in zeolites to the product distribution in the methanol-to-olefins process. ACS Catal 2024;14(15):11477–89.
[39] Zecchina A, Geobaldo F, Spoto G, Bordiga S, Ricchiardi G, Buzzoni R, et al. FTIR investigation of the formation of neutral and ionic hydrogen-bonded complexes by interaction of H-ZSM-5 and H-mordenite with CH_3CN and H_2O: comparison with the H-NAFION superacidic system. J Phys Chem 1996;100(41):16584–99.
[40] Wang C, Lu Y, Zhang Y, Fu H, Sun S, Li F, et al. Ru-based catalysts for efficient CO_2 methanation: synergistic catalysis between oxygen vacancies and basic sites. Nano Res 2023;16(10):12153–64.
[41] Song G, Li M, Yan P, Nawaz MA, Liu D. High conversion to aromatics via CO_2-FT over a CO-reduced Cu-Fe_2O_3 catalyst integrated with HZSM-5. ACS Catal 2020;10(19):11268–79.

[42] Zhou C, Shi J, Zhou W, Cheng K, Zhang Q, Kang J, et al. Highly active ZnO–ZrO_2 aerogels integrated with H-ZSM-5 for aromatics synthesis from carbon dioxide. ACS Catal 2020;10(1):302–10.
[43] Yang K, Li J, Wei C, Zhao Z, Liu Z. Coupling conversion of CO_2 and *n*-butane over modified ZSM-5: incorporation of the carbon from CO_2 into hydrocarbon products. ACS Catal 2023;13(15):10405–17.
[44] Gomez E, Nie X, Lee JH, Xie Z, Chen J. Tandem reactions of CO_2 reduction and ethane aromatization. J Am Chem Soc 2019;141(44):17771–82.
[45] Dai L, Zhou N, Li H, Wang Y, Liu Y, Cobb K, et al. Catalytic fast pyrolysis of low density polyethylene into naphtha with high selectivity by dual-catalyst tandem catalysis. Sci Total Environ 2021;771:144995.
[46] Lee HW, Park YK. Catalytic pyrolysis of polyethylene and polypropylene over desilicated beta and Al-MSU-F. Catalysts 2018;8(11):501.
[47] Li H, Hao C, Tian J, Wang S, Zhao C. Ultra-durable Ni–Ir/$MgAl_2O_4$ catalysts for dry reforming of methane enabled by dynamic balance between carbon deposition and elimination. Chem Catal 2022;2(7):1748–63.